Phonon local non-equilibrium at Al/Si interface from machine learning molecular dynamics

View Online   Export Citation   CrossMark

Krutarth Khot, (iD) Boyuan Xiao, Zherui Han, (iD) Ziqi Guo, (iD) Zixin Xiong, (iD) and Xiulin Ruan[a] (iD)

AFFILIATIONS

School of Mechanical Engineering and Birck Nanotechnology Center, Purdue University, West Lafayette, Indiana 47907, USA

[a]Author to whom correspondence should be addressed: ruan@purdue.edu

ABSTRACT

All electronics are equipped with metal/semiconductor junctions, resulting in resistance to thermal transport. The nanoscale phononic complexities, such as phonon local non-equilibrium and inelastic scattering, add to the computational or experimental characterization difficulty. Here, we use a neural network potential (NNP) trained by *ab initio* data, demonstrating near-first-principles precision more accurate than classical potentials used in molecular dynamics (MD) simulations to predict thermal transport at the Al/Si interface. The interfacial thermal conductance of $380 \pm 33 \, \text{MW/m}^2\text{K}$ from our NNP-MD simulations is in good agreement with the previous experimental consensus while considering the crucial physics of interfacial bonding nature, phonon local non-equilibrium, and inelastic scattering. Furthermore, we extract phonon mode insights from the NNP-MD simulations to reveal the decrease in local non-equilibrium of the longitudinal acoustic modes at the Al/Si interface. Our work demonstrates the utility of a machine learning MD to predict and extract accurate insights about interfacial thermal transport.

I. INTRODUCTION

Over the years, significant effort has gone into understanding and enhancing thermal transport across interfaces using theoretical and experimental techniques.[1–8] Critical understanding of the fundamental physics of interfacial heat transport across solid–solid interfaces is essential to design efficient electronics and energy devices. Interfacial thermal conductance (ITC) is the reciprocal of interfacial resistance (ITR), which relates the heat flux (Q) across a solid–solid interface with the temperature drop or jump (ΔT) at the interface, as shown in Fig. 1(a). In most dielectrics and semiconductors, the interfacial resistance is observed due to the scattering events of the lattice vibrations/phonons at the interface. Various computational methods have been developed to study the ITC and phonon dynamics, such as the acoustic mismatch model (AMM),[9] the diffuse mismatch model (DMM),[1] atomistic Green's function (AGF) method,[10] lattice dynamics (LD),[11] and molecular dynamics (MD).[12] The AMM and DMM consider specular and diffuse reflections of phonons at the interface, respectively. Recent developments have significantly improved the ITC prediction by considering the phonon local non-equilibrium at the interface.[13] However, DMM assumes elastic transport and neglects the interfacial bonding.[14]

Hence, significant room still exists to improve the prediction further. On the other hand, MD simulations include all higher-order lattice anharmonicity and phonon local non-equilibrium.

Theoretical frameworks have been developed based on equilibrium molecular dynamics (EMD) and non-equilibrium molecular dynamics (NEMD) to extract insights at the modal level in bulk materials and interfaces.[7,15–23] Insights from MD simulations reveal that anharmonicity can contribute significantly to ITC. Various MD studies on Si/Ge demonstrated nearly 15%–50% contribution of ITC from inelastic scattering.[20,23,24] These studies on semiconductor/semiconductor interfaces have enabled the optimization of ITC through a deeper understanding of nanoscale physics. In addition to semiconductor interfaces, a deeper understanding and characterization of the metal/semiconductor interfaces is essential for developing micro, nano, and quantum devices. NEMD simulations and experimental studies have been performed to understand thermal transport across such interfaces, such as Al/Si, Al/GaN, Cu/Si, and Al/SiO_2.[25–28] Al/Si is an important metal–semiconductor pair due to their prominence in electronic devices. ITC of the Al/Si interface has been studied over the years.[26,29–35] After many years of efforts, experimental measurements have achieved
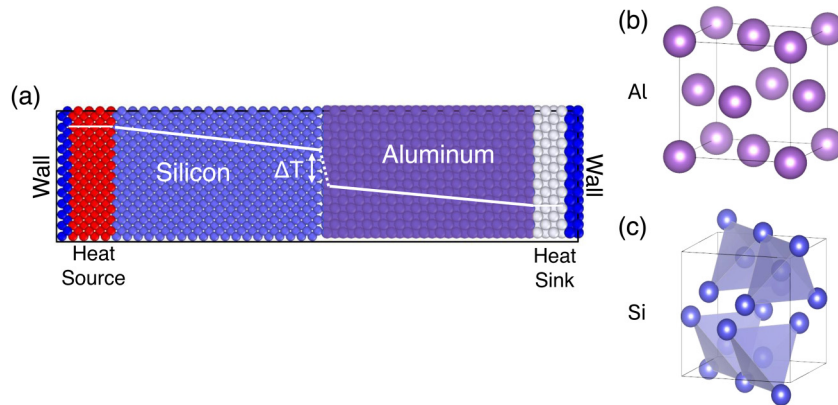
FIG. 1. (a) The Al/Si interface system illustrating the temperature profile and the interfacial temperature jump (ΔT) observed in non-equilibrium molecular dynamics (NEMD) simulations. (b) and (c) Atomic environments of the face-centered cubic (FCC) Al lattice and the diamond lattice type of Si, respectively.

consensus.[28,31,34,35] However, the simulation results and experimental measurements still show discrepancies with a lack of reliable theoretical explanation. Yang *et al.* used MD simulations based on the second nearest-neighbor modified embedded atom method (2NN MEAM) interatomic potential[36] to predict the ITC with and without electron–phonon coupling at the Al/Si interface.[25] The resulting ITC is over-predicted by ~20%–30% compared to the experimental measurements. Later, Xu *et al.* artificially matched the MD simulation's ITC with experiments by manually fitting a Lennard-Jones (LJ) function to the Al–Si interactions and investigated the role of anharmonicity at the interface.[26] Although the manually adjusted parameters improve agreement with experiments, such an approach may not necessarily capture the true nature of the atomistic interactions at the interface. As a result, these NEMD simulations for interfacial transport are limited by the empirical potentials used to describe atomic interactions. This limitation is especially pronounced across interfaces where certain mixing rules, such as arithmetic or geometric mean of the parameters, describe the interfacial interactions. This can lead to inaccurate or inconclusive characterization of the interfacial thermal transport. Additionally, unlike semiconductor–semiconductor junctions, where phonons are the majority heat carriers, metal–semiconductor junctions include the complexity of electron–phonon coupling from the metallic side.[25,29,37]

Using machine learning algorithms, data science methods have pushed the limits of understanding thermal physics by predicting and optimizing properties, such as lattice thermal conductivity and interfacial resistance.[38–41] Machine learning interatomic potential (MLIP) is an essential path to improve the accuracy of MD simulations. Behler and Parinello described the potential-energy surfaces (PESs) of materials using neural networks with density-functional theory (DFT) accuracy in 2007.[42] Subsequently, many ML techniques have been utilized to fit PES in the last two decades, such as neural network potential (NNP), Gaussian approximation potential (GAP), moment tensor potential (MTP), spectral neighbor analysis potential (SNAP), etc.[43–47] These potentials bridge the gap between first-principles accuracy accompanied by large computational costs and MD simulations that use empirical potentials. Various MLIPs have been developed and demonstrated specifically for phonon properties evaluation in recent

years.[48–57] MLIPs have been further used for interfacial thermal properties recently for Si/Ge,[58] Bi_2Te_3/Sb_2Te_3,[59] and MoS_2-WS_2.[57] Developing a MLIP is not trivial and the metal/semiconductor interface, such as Al/Si, further adds to the complexity due to their significantly different atomic environments, interactions, and material properties.

Here, we demonstrate the development of an NNP to predict phonon properties at the metal/nonmetal interfaces with first-principles accuracy and provide phonon spectroscopy insights using Al/Si as a prototype system. In addition to the interfacial interactions, our NNP provides a unique novelty through its ability to predict the atomic interactions in two distinct atomic environments—a face-centered cubic (FCC) lattice of metallic Al and a diamond cubic lattice of non-metallic Si, as shown in Figs. 1(b) and 1(c), respectively. Our NNP-NEMD simulations are able to include three critical factors of interfacial thermal transport—an accurate description of interfacial bonding, phonon local non-equilibrium, and inelastic transport. Previous Landauer-approach-based studies often do not entirely capture these effects, while MD simulations with empirical potentials are inaccurate and inconclusive. The resulting ITC from our NNP-NEMD simulations is in good agreement with the recent experimental consensus while capturing the *ab initio* nature of interfacial bonding between Al and Si. Additionally, we decompose the atomic trajectories to obtain spectral insights into the interfacial behavior of phonons and demonstrate the presence of very thin interfacial regions and strong phonon local non-equilibrium in the Al/Si system.

II. METHODOLOGY

A. Development of neural network potential

First, we generate the training dataset comprising atomic trajectories, energies, and forces for the bulk phases of the two materials and the interface supercell of Al/Si using AIMD simulations. All the first-principles calculations are based on DFT as implemented in the Vienna *Ab Initio* Simulation Package (VASP).[60,61] We use the projector augmented wave (PAW) pseudopotentials and generalized gradient approximations of the Perdew–Burke–Ernzerhof (PBE) exchange-correlation functional.[62,63] Three supercells—bulk Al FCC, diamond cubic Si, and Al/Si interface—are used to build

TABLE I. Details for training dataset generation.

System	No. of atoms	Type	Temperatures (K)	Frames
Bulk Al	320	AIMD	50, 100, 200, 300, 400, 500	3000
Bulk Si	128	AIMD	50, 100, 200, 300, 400, 500	3000
Al/Si interface	408	AIMD	50, 100, 200, 300, 400, 500	1500
Test set (bulk Al)	320	AIMD	50–500 (with intermediate ramps)	1000
Test set (bulk Si)	128	AIMD	50–500 (with intermediate ramps)	1000
Test set (Al/Si interface)	408	AIMD	50–500 (with intermediate ramps)	2000

the dataset. Our input supercells' initial lattice constants for aluminum and silicon are 4.04 Å and 5.43 Å, respectively. We pair 4×4 Al unit cells with 3×3 Si unit cells to match the cross-sectional area and reduce interfacial strain. We perform AIMD simulations at finite temperatures (50, 100, 200, 300, 400, and 500 K) using the isobaric–isothermal ensemble for each supercell for 3 ps with a time step of 1 fs. Additionally, we generate a test dataset using AIMD simulations for the bulk Al, bulk Si, and Al/Si interface supercell in the same temperature range. The test dataset also includes AIMD simulations with temperature ramps to test the neural network's predictions at intermediate temperatures. The details of these datasets are shown in Table I.

The NNP is trained using the Smooth Edition of Deep Potential (DeePot-SE) from DeePMD package.[46,64] Our NNP is constructed using a 3-layer embedding net with 32–64–128 nodes and a 3-layer fitting net with 128 nodes in each layer, utilizing the tanh activation function. The fitting net maps the embedded inputs to the atomic energies and forces. The interaction cutoff radius is 6.0 Å with smoothening at 5.6 Å. The model is trained for 2×10^6 steps, with a batch size of 2, a starting learning rate of 1×10^{-3}, and a decay rate of 0.98. The prefactors for the energy and force loss contributions to the loss function were set as $p_e^{start} = 0.1$, $p_e^{limit} = 10$, $p_f^{start} = 1000$, and $p_f^{limit} = 1$. Further mathematical details of the neural network algorithms can be found in the literature.[46,64] The crucial hyperparameters were tuned using various model architectures shown in Figs. S1–S4 of the supplementary material. The selected hyperparameters demonstrated reasonable computing cost and prediction accuracy. Figure S5 in the supplementary material shows the evolution of the loss function for the final model architecture during the NNP training. The trained model and dataset are available online.[65]

B. Simulation setup

The MD simulations are performed using the Large-Scale Atomic/Molecular Massively Parallel Simulator (LAMMPS) package[66,67] using the trained Al/Si NNP. We use the NEMD framework in LAMMPS, which utilizes Fourier's law to evaluate the heat transport across the system. In this method, we set the two ends of the system as a heat sink and heat source using a Langevin thermostat. As described earlier, for dataset generation, it is essential to reduce strain at the interface. The MD input structure is built with a 8×8 unit cell cross section of Al with a 6×6 unit cell cross section of Si. The time step for the MD simulations is set as 0.5 fs, which is short enough to resolve all the phonon modes. All NEMD

runs follow a common equilibration strategy, which starts with an isobaric–isothermal (NPT) ensemble at 0 Pa and 300 K. This allows the system to equilibrate considering the thermal expansion. Next, we switch to the constant temperature and volume (NVT) ensemble. Finally, we use the constant energy and temperature (NVE) ensemble. We perform the NPT, NVT, and NVE for 250 ps each. The ends of the simulation box in the x-direction are frozen to set them as walls. We set up a temperature gradient using the Langevin thermostat using reservoirs at the ends next to the walls, as shown in Fig. 1(a). Silicon is used as the heat source and aluminum as the heat sink, as semiconductors are often the heat source in electronic devices. A temperature gradient of ± 30 K is generated using the Si source at 330 K and the Al sink at 270 K. The heat current and the corresponding temperature profile are allowed to stabilize for about 250 ps before collecting the data for the last 100 ps of the NEMD simulation.

The ITC (G) is calculated from the temperature jump (ΔT) across the interface using the relation

$$G = \frac{J}{A\Delta T}, \qquad (1)$$

where J is the heat flux across the cross-sectional area (A) for the system. The linear regions of the temperature profile are fitted with a straight line to extract the temperature jump at the interface and calculate the ITC.

C. Spectral phonon method

The temperatures for different phonon modes can be calculated from the NEMD simulations based on the bulk eigenvector of the material. The formalism was first developed by Zhou *et al.*[19] for modal heat fluxes and later extended by Feng *et al.*[21,23] to calculate the modal temperatures. Here, we briefly discuss the calculation methodology for the modal temperatures using the time derivative of the normal mode amplitude ($\dot{\Phi}(t)$). $\dot{\Phi}(t)$ can be obtained using the eigenvectors and trajectory information as

$$\dot{\Phi}_\lambda(t) = \frac{1}{\sqrt{N_c}} \sum_{l,b}^{N_c,n} \sqrt{m_b} \exp(-ik \cdot r_{l,b}^0) e_{b,\lambda}^* \cdot \dot{u}_{l,b}(t), \qquad (2)$$

where l and b are the indices of the primitive cells and basis atoms. N_c and n are the total number of primitive cells and atoms. m, r^0, and $\dot{u}$ are the mass, coordinates, and velocity vector of the atom,

respectively. k is the phonon wavevector, and $e_{b,\lambda}^*$ is the complex conjugate of the eigenvector at the basis atom b for the phonon mode λ. The modal temperature (T_λ) at mode λ is obtained using the time derivative of the normal mode amplitude as

$$T_\lambda = \langle \dot{\Phi}_\lambda^*(t)\dot{\Phi}_\lambda(t) \rangle / k_B, \tag{3}$$

where the angle brackets refer to time averaging to eliminate MD fluctuations and k_B is the Boltzmann constant. The phonon normal mode temperature effectively represents the carrier energy density under non-equilibrium conditions. Further details of this method can be found in the literature.[21] The input data of atomic coordinates and velocities are obtained from the LAMMPS NEMD simulations using $8 \times 8 \times 8$ Al cells and $6 \times 6 \times 6$ Si cells. The eigenvectors are obtained using lattice dynamics calculations using the Al/Si NNP in Phonopy.[68,69]

III. RESULTS AND DISCUSSION

A. NNP validation

Following the training, we evaluate the accuracy of the trained NNP using our test dataset. The energies and forces predicted by the NNP are compared with the AIMD energies and forces in Figs. 2(a) and 2(b), respectively. The NNP predicted quantities agree well with the *ab initio* quantities in the 50–500 K temperature range. The accuracy of the per-atom forces in the Al/Si supercell demonstrates the NNP's capability to predict the interfacial interactions of Al and Si. We quantify the accuracy using the root-mean-square error (RMSE) for energy and forces as

$$RMSE_{energy} = \sqrt{\sum_{i=1}^{n} \frac{(E_{i,NNP} - E_{i,AIMD})^2}{n}}, \tag{4}$$

$$RMSE_{force} = \sqrt{\sum_{i=1}^{n} \frac{(F_{i,NNP} - F_{i,AIMD})^2}{n}}, \tag{5}$$

where n is the number of test points used for the evaluation. The per-atom energy RMSE for our NNP is 0.55, 0.21, and 0.53 meV/atom for the bulk Al, bulk Si, and Al/Si supercell test sets, respectively. The force RMSE is 0.028, 0.020, and 0.047 eV/Å for the bulk Al, bulk Si, and Al/Si supercell test sets, respectively. Our RMSE values are within the acceptable range for NNP. Previous investigations on MLIPs report that an energy error of the order of 1 meV/atom is expected in MLIPs.[52] Our NNP's prediction accuracy holds further significance due to the presence of bulk and interface regions of Al and Si atom types. Furthermore, we also compare the prediction error from the classical potentials with the AIMD test dataset using the combination of embedded atom method (EAM)[70] for Al–Al, manually fitted LJ[26,71] for Al–Si, and Tersoff potential[72] for Si–Si utilized most recently to understand the Al/Si interfacial thermal transport.[26] The $RMSE_{energy}$ is 783.39 meV/atom, and $RMSE_{force}$ is 1.59 eV/Å for the Al/Si test dataset. This large mismatch in a classical potential and DFT calculation further justifies the development and use of our NNP to characterize and study thermal transport at a metal/nonmetal interface.

Next, in Figs. 2(c)–2(f), the harmonic phonon properties of Al and Si are calculated using DFT, classical potentials, and our NNP using lattice dynamics calculations. Experimental phonon dispersion obtained from the literature[73,74] alongside DFT results are used as a benchmark comparison. The MEAM and EAM potentials are used for Al, while Tersoff and Stillinger–Weber potentials are used for Si for comparison. The choice of potentials is inspired by recent MD studies on Al/Si interfacial thermal transport.[25,26] The LAMMPS interface with Alamode calculates the second-order force constants required for obtaining the dynamical matrix.[66,75] Figures 2(c) and 2(d) show the phonon dispersion, whereas Figs. 2(e) and 2(f) show the phonon density of states (PDOS) for Al and Si, respectively. The MEAM potential for Al overestimates the acoustic branches significantly. The EAM potential is slightly better than MEAM; however, it still deviates significantly from the benchmark. The dispersion curves from NNP for Al are in reasonably good agreement with the experimental[74] and DFT results. In Si, the Tersoff potential softens the acoustic branches, while the SW potential hardens them, as shown in Fig. 2(d). Both potentials also show significant hardening of the optical branches with cutoff frequencies >15 THz, which is not the case in the experimental results[73] and the DFT-calculated dispersion. Thus, classical MD simulations often compromise the accuracy of harmonic properties, which can lead to unreliable characterization of the ITC. Meanwhile, the NNP-based phonon dispersion agrees well with the experiment and the DFT benchmark. Our NNP demonstrates remarkable capability to accurately predict the harmonic phonon properties in two distinctly different atomic environments. This prediction accuracy of harmonic properties alongside the Al/Si interfacial interaction predictions trained using *ab initio* data creates a reliable pathway for evaluating the ITC. In addition to the challenges faced in developing the earlier interfacial MLIPs for Si/Ge,[58] Sb$_2$Te^3/Bi$_2$Te^3,[48] and MoS$_2$-WS$_2$,[57] the Al/Si system faces the unique challenge of predicting the properties of a metal and a nonmetal using the same neural network. We overcome this tricky challenge for the Al/Si interface using the additional AIMD dataset of the bulk materials and fine-tuning the NNP training process. Furthermore, Fig. S6 in the supplementary material presents the radial distribution function of Al and Si from the NNP-MD simulations at room temperature, demonstrating a good agreement of crystallinity with established empirical potentials.

B. Interfacial thermal conductance

After validating the accuracy of our NNP on all fronts, the NEMD simulations are performed for the Al/Si interface. The temperature profile in both Al and Si is fit linearly to obtain the temperature jump across the interface given by ΔT_{fit}, as shown in Fig. 3(a). The ITC obtained from NEMD simulations is known to be limited by the size effects due to finite system size.[33] As the ends of the simulation box are fixed, as shown in Fig. 1(a), phonons of the mean free path larger than the box size are not captured in the simulation. Hence, we observe the size effects, which affect the ITC values. Shelling *et al.* proposed using the finite size resistances to extrapolate it for infinite size,[76] and it is demonstrated for the Al/Si
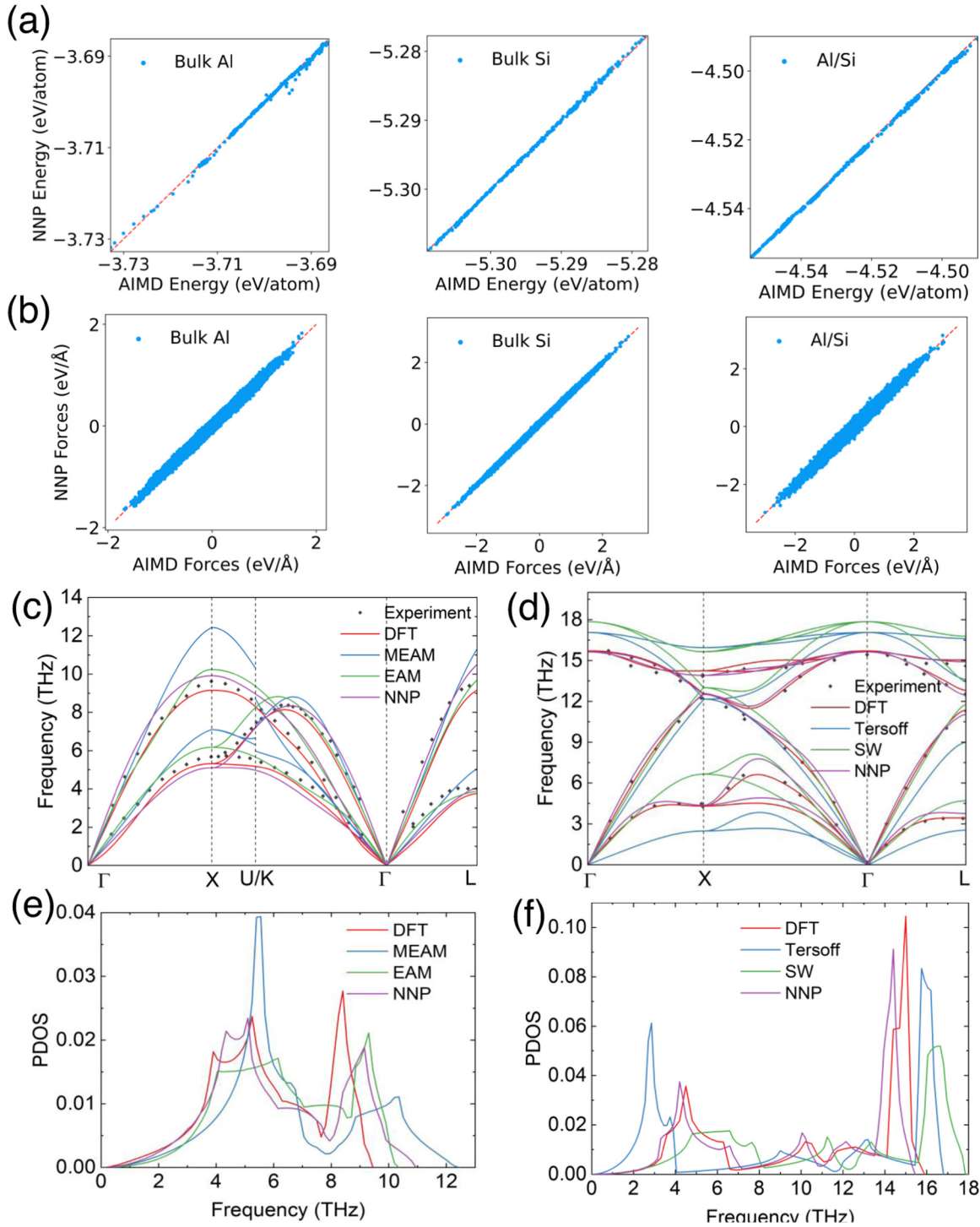
FIG. 2. (a) Comparison of energies predicted by the NNP vs the *ab initio* energy from the test dataset for bulk Al, bulk Si, and Al/Si interfacial subsystems, respectively. (b) Comparison of forces predicted by the NNP vs the *ab initio* forces from the test dataset for bulk Al, bulk Si, and Al/Si interfacial subsystems, respectively. (c) and (d) Phonon dispersion curves from experimental data, DFT, classical potentials, and NNP for Al and Si, respectively. Experimental data of Al and Si are extracted from Refs. 65 and 66, respectively. (e) and (f) Phonon density of states calculated using DFT, classical potentials, and NNP for Al and Si, respectively.
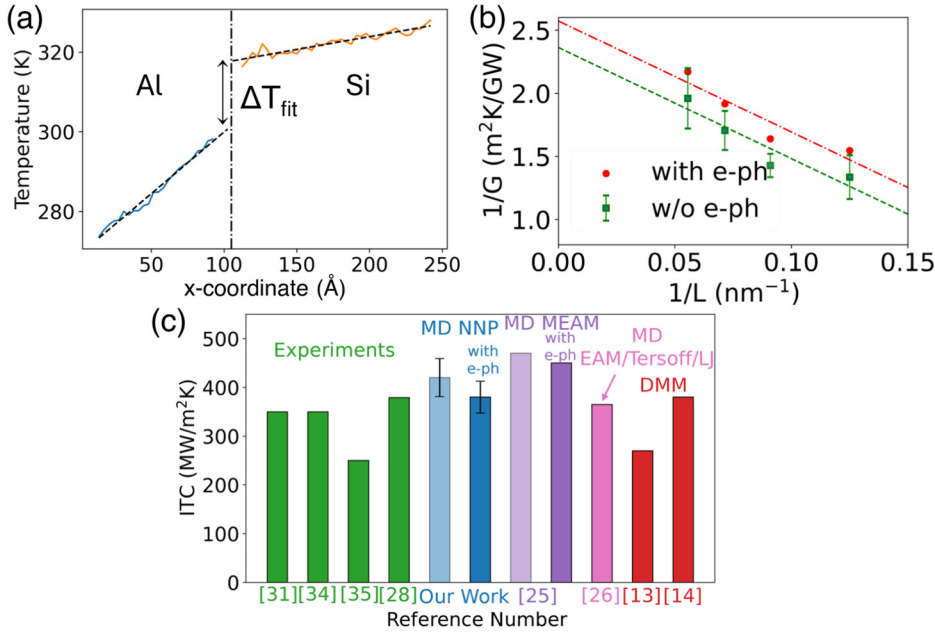
FIG. 3. (a) Linear fit applied in the bulk regions of both Al and Si, which is extrapolated to the interface to obtain the ΔT_{fit} for the ITC calculation. (b) Interfacial thermal resistance (1/G) as a function of the inverse of length (1/L) at room temperature for an Al/Si system with and without electron–phonon coupling calculated using NEMD simulations assisted by the trained NNP. (c) Comparison of experimental measurements of Al/Si ITC[28,31,34,35] with our NNP-MD ITC predictions and previously reported MD simulations using MEAM 2NN, EAM–Tersoff–LJ potentials,[25,26] and the diffuse mismatch model,[13,14] respectively.

interface by Yang et al.[25] The formulation for extrapolating the ITC is given as follows:

$$\rho(\infty) = \rho(L) + \frac{C}{L}, \quad (6)$$

where $\rho(L)$ is the interfacial resistance at some length L, and C is a constant. This equation can be converted to interfacial conductance (G) as

$$\frac{1}{G(\infty)} = \frac{1}{G(L)} + \frac{C}{L}. \quad (7)$$

We follow this approach in our work to obtain the interfacial conductance of the Al/Si interface for an infinite system. Additionally, previous studies have shown that electron–phonon coupling at the interface due to electrons from aluminum reduces the ITC.[25,37] We correct the ITC values by considering the electron–phonon coupling contribution using the series resistance model suggested by Majumdar and Reddy[37] as follows:

$$\frac{1}{G} = \frac{1}{G_{eph}} + \frac{1}{G_{pp}}, \quad (8)$$

where G_{ep} and G_{pp} are the interfacial conductance due to electron–phonon and phonon–phonon interactions, respectively. G_{pp} is obtained from the NEMD simulation, where G_{ep} is calculated as

$$G_{ep} = \sqrt{g_{Al} \kappa_{ph,Al}}, \quad (9)$$

where g_{Al} is the electron–phonon coupling parameter for aluminum, which is found from the literature to be 2.45×10^{17} W/m^3−K^{-1}[77,78]

and $\kappa_{ph,Al}$ is the phononic thermal conductivity of aluminum. The $\kappa_{ph,Al}$ is reported to be around 9.5 W − m^{-1}K^{-1} obtained from first-principles calculations.[79,80] The infinite conductance model, along with the electron–phonon coupling model, together serves as an efficient tool to estimate the overall ITC for the Al/Si system.

Figure 3(b) shows the inverse of interfacial conductance obtained from NEMD simulations for a finite size against the inverse of a domain size. We observe the interfacial conductance decreases with increasing system size. ITC for infinite size without electron–phonon coupling reaches 420 ± 39 MW/m^{2}K. When the electron–phonon coupling contribution is included, the ITC decreases slightly to 380 ± 33 MW/m^{2}K at a room temperature of 300 K. This is due to an additional scattering mechanism acting as a resistance to the heat current. Our results show a 9.5% decrease in ITC due to aluminum electrons. In Fig. 3(c), the ITC values are compared with the previously reported experimental measurements[28,31,34,35] and computational simulations[13,14,25,26] performed at room temperature. In the last decade, experiments have agreed to the ITC of about 350 MW/m^{2}K for the Al/Si interface.[28,31,34,35] Among these, the time-domain thermoreflectance (TDTR) measurement at an atomically sharp Al/Si interface shows a thermal conductance of 379 MW/m^{2}K.[28] Our NNP-NEMD ITC of 380 MW/m^{2}K agrees well with the overall experimental consensus. Classical MD simulations using the MEAM 2NN potential overestimate the ITC by 20%–30%, while the LJ potential used by Xu et al. is manually fitted to agree with the experimental ITC. The natural agreement of NNP-NEMD-based ITC exemplifies the utility and accuracy of ML potentials to characterize and quantify interfacial thermal transport. Furthermore, our ITC value of 380 MW/m^{2}K is similar to the non-equilibrium Landauer approach coupled with DMM by Shi et al.,[13] which improves on the original DMM by considering the phonon local non-equilibrium in their model.

However, as DMM still does not consider interfacial bonding and inelastic scattering, this could be a coincidental agreement enabled by some canceling errors in the calculation. This makes our NNP-NEMD approach the most accurate method to quantify the ITC at the metal/non-metal Al/Si interface. This approach captures all higher-order scattering processes, utilizes the interfacial bonding with first-principles accuracy, and considers the phonon local non-equilibrium. Furthermore, we also include the corrections to consider size effects and electron–phonon coupling using the earlier discussed methodologies.

C. Spectral analysis

To further understand the underlying physics, the density of vibrational states must be analyzed from the different regions of the NEMD simulation system. Fourier transform of autocorrelated atomic velocities is used to obtain the phonon density of states (PDOS) from the NNP-NEMD simulations. In Fig. 4(a), we show the PDOS in the bulk and near-interface regions of the Al/Si system. The top panel shows the bulk region of Al with a cutoff vibrational frequency of ~10 THz. However, as shown in the bottom panel, bulk Si has optical phonon modes concentrated in the $12 < \omega < 16$ THz range. This bulk PDOS gets affected closer to the interface. The PDOS of layer 1 captures the vibrational modes of a single atomic layer of Al and Si in direct contact at the interface, which we refer to as the "interfacial region." Si dumps its

optical phonon energy in the $12 < \omega < 16$ THz band to a lower frequency range in this interfacial region suitable for energy transfer into the Al interfacial region. This creates a pathway for thermal transport across the interface. Some modes are activated in Al at $\omega > 10$ Thz, but these are limited to the interfacial region. These modes arise from the optical phonons of Si. As optical phonon branches are absent in Al, the vibrational modes of $\omega > 10$ THz vanish quickly as we move away from the interfacial region. On the contrary, the Al/Si system described by the MEAM 2NN potential shows Si vibrational modes in the frequency range of 15–20 THz near the interface,[25] as shown in Fig. 4(b). In principle, this should not be the case, and it can be accounted as an artifact of the classical potential used to define interfacial bonding. Our NNP provides *ab initio* accuracy for interfacial interactions, which overcomes the caveat of mixing rules used in classical MD simulations. The intuitive shift of Si phonon modes toward lower frequency is more distinct in NNP-NEMD simulations compared to previous classical potential NEMD simulations.

Furthermore, Feng *et al.* have suggested that a smaller difference in atomic masses allows the lighter atom to affect the heavier atoms' vibrational modes at the interface.[23] In our case, the atomic mass of Al and Si is 26.98 and 28.85 amu, respectively. Due to the small mass difference, Al vibrational modes can pull the Si modes to a lower frequency to facilitate thermal transport. This corresponds to the reduced phonon density in the Si interface layer's $12 < \omega < 16$ THz region. Differences in interfacial phonon modes
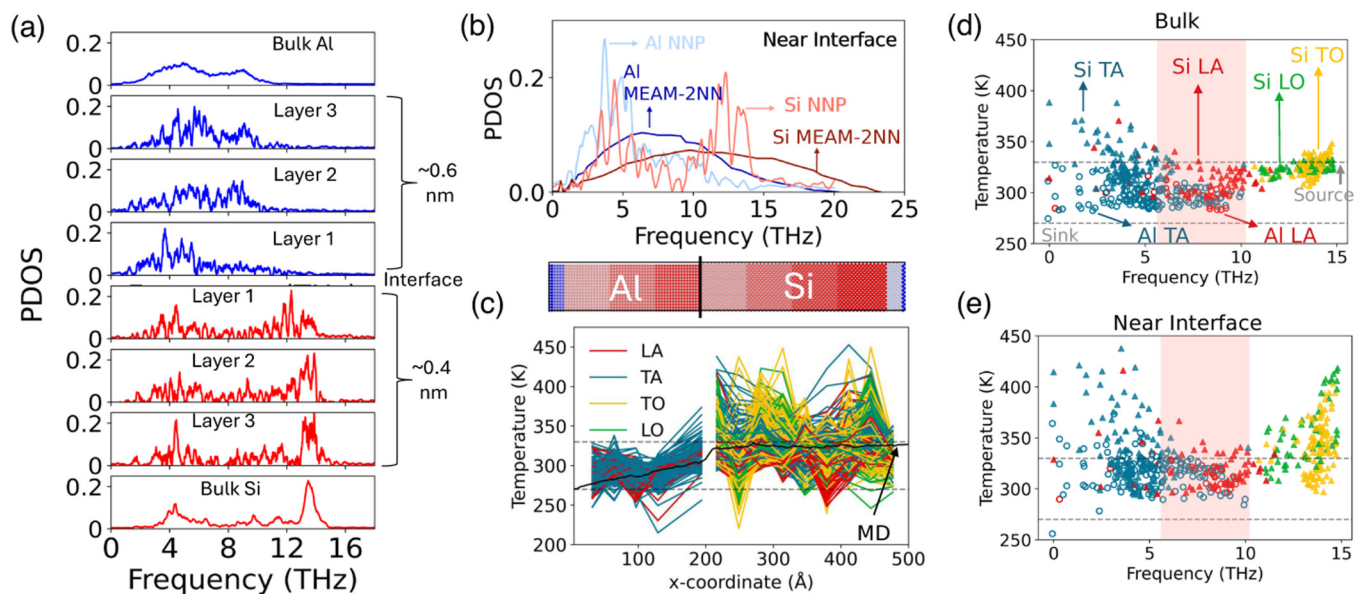

FIG. 4. (a) Phonon density of states (PDOS) at different locations of the Al/Si simulation domain. The top four panels are Al and the bottom four panels are Si. The top and bottom panel shows the bulk region PDOS, while the three central panels of both Al and Si show the PDOS of atomic layers in closest contact with the interface. (b) Standardized PDOS comparison for Al and Si atoms near the interface using NNP and MEAM-2NN potential in NEMD simulation at 300 K. MEAM-2NN potential PDOS extracted from Ref. 25. (c) Phonon temperatures in Al and Si as a function of the x-coordinate. The illustration on the top shows that the Al/Si domain is divided into smaller boxes for modal decomposition. The solid line shows the actual MD temperature profile, and the dashed lines show the heat source and the heat sink temperature. (d) and (e) Phonon temperatures in Al and Si as a function of frequency for the bulk domains that are not in contact at the interface and the near-interface domain, respectively. The highlighted band illustrates the thermal pathway created by the LA modes of Al.

compared to bulk phonon modes were first shown by Gordiz and Henry.[7,20] They demonstrated that the phonon modes at the interface are dissimilar to the bulk modes and contribute to enhancing the ITC. Later, Feng *et al.* presented a conflicting argument where they proposed that the interfacial modes are limited to only a few layers of about 0.5 nm in an Si/Ge system.[23] As a result, the interface can be considered a thin boundary where bulk modes from material A are transported to material B. In the Al/Si interface, the NNP-NEMD demonstrates interfacial modes limited to a few atomic layer-sized interfacial region. The Al and Si atoms recover the bulk vibrational modes at less than 1 nm from the interface. Our work using the NNP-NEMD thoroughly validates the findings of Feng *et al.* using classical MD through the NNP's *ab initio* accuracy of interfacial interactions.

In addition to the interfacial modes, the inelastic or anharmonic phonon scattering and the phonon local non-equilibrium are crucial to interfacial thermal transport. Xu *et al.* have previously analyzed and quantified the anharmonic phonon scattering contribution, which is about ∼25% at room temperature.[26] A detailed analysis of the phonon local non-equilibrium is not yet reported. Combined with NNP-NEMD, which includes all elastic and inelastic scattering events predicted at first-principles accuracy, a spectral temperature analysis is the most realistic and reliable pathway for observing the phonon local non-equilibrium present at the Al/Si metal/semiconductor interface. Here, we decompose the atomic trajectories from the NNP-NEMD simulations to obtain the modal temperatures in Al and Si using the spectral phonon temperature method.

The spectral temperature can be understood as the carrier energy density of a particular vibrational mode. In Fig. 4(c), the top graphic displays the Al/Si simulation box of ∼30 000 atoms used for the decomposition. Although our NNP-NEMD domain is slightly smaller than previous classical MD studies,[23,81] it falls within the limits of the dominating phonon modes of Al and Si at room temperature.[80,82] The spatial variations in branch temperatures of Al and Si in the heat flux direction of our NEMD simulation are shown in Fig. 4(c). These modes are classified depending on their branch type, i.e., transverse acoustic (TA), longitudinal acoustic (LA), transverse optical (TO), and longitudinal optical (LO). In Al, the phonon temperatures increase near the interface, indicating the energy accumulated from interfacial Si atoms. In Si, the optical modes and some TA modes are at higher temperatures near the interface, while the LA phonon modes are close to the average MD temperature. This demonstrates a higher local non-equilibrium between the Al phonons and the optical and some transverse acoustic phonons of Si.

Phonon non-equilibrium reduces the conductance of the acoustic phonons, which are the effective heat carriers, and increases the conductance of the non-effective optical phonon heat carriers.[23] To gain more clarity on the phonon local non-equilibrium at the modal level, we compare the difference in phonon temperatures in the bulk region vs the near-interface region. In Figs. 4(d) and 4(e), the modal temperatures are plotted against the frequency of the modes for the bulk region (away from the interface) and the near-interface region, respectively. As observed in Fig. 4(d), in Al, the bulk region LA modes in the frequency range of 5–10 THz are at a lower temperature of around

280 K. These Al LA phonons show temperatures in the range of 300–320 K near the interface. Meanwhile, the Si LA phonons are in the same temperature range. This reduces the local non-equilibrium between the Si and Al LA modes. The reduced local non-equilibrium in the 5–10 THz band of effective heat carriers, in addition to the overlapping density of states, as observed in Fig. 4(b), enables energy transfer across the Al/Si interface. Furthermore, the LO phonons of Si in the 10–12 THz range are also at similar temperatures of 300–320 K near the interface, creating another gateway to Al LA modes through inelastic scattering. In Fig. 4(e), the band highlighting the phonon modes in Al and Si illustrates the stronger thermal transport pathway. Previous classical MD simulations also suggest that phonon modes at $\omega < 10$ THz are the major energy carriers at the Al/Si interface.[26]

As observed in Fig. 4(a), the higher frequency optical phonons (12 THz $< \omega <$ 16 THz) of Si pass their energy to lower frequencies through inelastic scattering. This allows the phonon modes in Al to receive energy across the interface from the Si LA and LO modes in the modal vicinity. Additionally, as Al does not have optical phonon modes, the high-frequency optical phonons (12 THz $< \omega <$ 16 THz) in Si, despite exhibiting significant non-equilibrium, do not contribute directly to the interfacial conductance. Thus, our spectral analysis demonstrates the phonon local non-equilibrium at the interface using the near-first-principles accuracy of interfacial bonding enabled by the NNP-NEMD simulations.

The utility and accuracy demonstrated by our Al/Si NNP model further highlight the scope of ML-based interatomic potentials to investigate and discover complex physics, such as interfacial thermal transport with near-first-principles accuracy. An identical training methodology can be used to develop NNP models for other metal/semiconductor interfaces relevant to future electronic devices. It can also be extended to broader conditions, including higher temperatures, varied pressures, and different material phases, by incorporating additional datasets built using AIMD simulations in the targeted conditions. However, expanding the training dataset increases computational costs, requiring more complex neural network architectures that slow down the MD simulations. Thus, achieving a balance between accuracy, universality, and computational efficiency is crucial to ensure practical and effective simulations.

IV. CONCLUSION

In summary, we develop a neural network potential (NNP) for the Al/Si metal/semiconductor interface to estimate and further understand the interfacial thermal transport. The NNP is trained and tuned to accurately predict thermal properties for face-centered cubic Al, diamond cubic Si, and the Al/Si interface using *ab initio* datasets. Non-equilibrium molecular dynamics (NEMD) simulations are performed using the comprehensive accuracy in bulk and interfacial facets provided by the NNP. The interfacial thermal conductance (ITC) is extracted by employing simplified models to eliminate size effects and include the electron–phonon contribution arising from the metal. The NNP-NEMD results show an ITC of 420 MW/m² K, which reduces by ∼10% to 380 MW/m² K when the electron–phonon coupling is considered. Our ITC values show

agreement with the recent experimental consensus, which was missing in previous classical MD results reported in the literature. This illustrates the utility of our NNP, enabling enhanced accuracy of MD simulations. Moreover, the atomic trajectories from the NNP-NEMD simulations are decomposed to extract spectral insights at the interface. The phonon density of states shows the presence of interfacial modes in a very thin atomic layer region limited to ~0.5 nm from the interface where Si atoms vibrate closer to the ~10 THz cutoff frequency of Al. Our spectral phonon temperature analysis demonstrates the phonon local non-equilibrium in the phonon modes of Al and Si in the near-interface region using near-first-principles-accuracy of NNP-NEMD simulations. Our work offers a novel, reliable, and accurate pathway to develop an NNP to predict thermal properties for distinct materials, such as Al and Si, and their interface with state-of-the-art accuracy. These results significantly advance the accuracy and understanding of thermal transport at the metal/nonmetal interface through insights obtained from NNP-based molecular dynamics simulations.

SUPPLEMENTARY MATERIAL

See the supplementary material that includes hyperparameter tuning for neural network training, evolution of the loss function of neural network potential, and a radial distribution function (RDF) comparison of NNP and classical potentials in MD simulations.

AUTHOR DECLARATIONS

Conflict of Interest

The authors have no conflicts to disclose.

Author Contributions

X.R. conceived the study. K.K. developed the dataset and codes, performed simulations, and investigated the results. K.K. and B.X. trained the model. Z.H., Z.G., and Z.X. helped with the analysis. X.R. supervised the project. All authors contributed to discussions and revisions of the manuscript.

Krutarth Khot: Data curation (equal); Formal analysis (equal); Investigation (equal); Methodology (equal); Visualization (equal); Writing – original draft (equal); Writing – review & editing (equal). **Boyuan Xiao:** Data curation (equal); Writing – review & editing (equal). **Zherui Han:** Writing – review & editing (equal). **Ziqi Guo:** Writing – review & editing (equal). **Zixin Xiong:** Writing – review & editing (equal). **Xiulin Ruan:** Conceptualization (equal); Formal analysis (equal); Funding acquisition (equal); Supervision (equal); Writing – review & editing (equal).

DATA AVAILABILITY

The data that support the findings of this study are available from the corresponding author upon reasonable request.

REFERENCES

[1]E. T. Swartz and R. O. Pohl, "Thermal boundary resistance," Rev. Mod. Phys. **61**, 605 (1989).

[2]D. G. Cahill, W. K. Ford, K. E. Goodson, G. D. Mahan, A. Majumdar, H. J. Maris, R. Merlin, and S. R. Phillpot, "Nanoscale thermal transport," J. Appl. Phys. **93**, 793–818 (2003).

[3]L. Hu, L. Zhang, M. Hu, J. S. Wang, B. Li, and P. Keblinski, "Phonon interference at self-assembled monolayer interfaces: Molecular dynamics simulations," Phys. Rev. B: Condens. Matter Mater. Phys. **81**, 235427 (2010).

[4]R. Cheaito, J. T. Gaskins, M. E. Caplan, B. F. Donovan, B. M. Foley, A. Giri, J. C. Duda, C. J. Szwejkowski, C. Constantin, H. J. Brown-Shaklee, J. F. Ihlefeld, and P. E. Hopkins, "Thermal boundary conductance accumulation and interfacial phonon transmission: Measurements and theory," Phys. Rev. B: Condens. Matter Mater. Phys. **91**, 035432 (2015).

[5]Z. Tian, K. Esfarjani, and G. Chen, "Enhancing phonon transmission across a Si/Ge interface by atomic roughness: First-principles study with the Green's function method," Phys. Rev. B: Condens. Matter Mater. Phys. **86**, 235304 (2012).

[6]T. Luo and G. Chen, "Nanoscale heat transfer—From computation to experiment," Phys. Chem. Chem. Phys. **15**, 3389–3412 (2013).

[7]K. Gordiz and A. Henry, "A formalism for calculating the modal contributions to thermal interface conductance," New J. Phys. **17**, 103002 (2015).

[8]B. Shi, X. Tang, T. Lu, T. Nakayama, Y. Li, and J. Zhou, "Interfacial thermal conductance at metal-nonmetal interface via electron-phonon coupling," Mod. Phys. Lett. B **32**, 32 (2018).

[9]I. Khalitnikov, "Heat exchange between a solid body and helium—I," Zh. Eksp. Teor. Fiz. **22**, 687–704 (1952).

[10]J. S. Wang, J. Wang, and N. Zeng, "Nonequilibrium Green's function approach to mesoscopic thermal transport," Phys. Rev. B: Condens. Matter Mater. Phys. **74**, 033408 (2006).

[11]D. A. Young and H. J. Maris, "Lattice-dynamical calculation of the Kapitza resistance between fcc lattices," Phys. Rev. B **40**, 3685 (1989).

[12]A. Maiti, G. D. Mahan, and S. T. Pantelides, "Dynamical simulations of non-equilibrium processes—Heat flow and the Kapitza resistance across grain boundaries," Solid State Commun. **102**, 517–521 (1997).

[13]J. Shi, X. Yang, T. S. Fisher, and X. Ruan, "Dramatic increase in the thermal boundary conductance and radiation limit from a nonequilibrium Landauer approach," arXiv:1812.07910 (2019).

[14]P. Reddy, K. Castelino, and A. Majumdar, "Diffuse mismatch model of thermal boundary conductance using exact phonon dispersion," Appl. Phys. Lett. **87**, 211908 (2005).

[15]Y. Chalopin and S. Volz, "A microscopic formulation of the phonon transmission at the nanoscale," Appl. Phys. Lett. **103**, 051602 (2013).

[16]Y. Chalopin, A. Rajbpour, H. Han, Y. Ni, and S. Volz, *Annual Review of Heat Transfer* (Begel House, Inc., 2014), Vol. 17, pp. 147–176.

[17]K. Sääskilahti, J. Oksanen, J. Tulkki, and S. Volz, "Role of anharmonic phonon scattering in the spectrally decomposed thermal conductance at planar interfaces," Phys. Rev. B **90**, 134312 (2014).

[18]K. Sääskilahti, J. Oksanen, J. Tulkki, and S. Volz, "Spectral mapping of heat transfer mechanisms at liquid-solid interfaces," Phys. Rev. E **93**, 052141 (2016).

[19]Y. Zhou, X. Zhang, and M. Hu, "Quantitatively analyzing phonon spectral contribution of thermal conductivity based on nonequilibrium molecular dynamics simulations. I. From space Fourier transform," Phys. Rev. B **92**, 195204 (2015).

[20]K. Gordiz and A. Henry, "Phonon transport at interfaces: Determining the correct modes of vibration," J. Appl. Phys. **119**, 28 (2016).

[21]T. Feng, W. Yao, Z. Wang, J. Shi, C. Li, B. Cao, and X. Ruan, "Spectral analysis of nonequilibrium molecular dynamics: Spectral phonon temperature and local nonequilibrium in thin films and across interfaces," Phys. Rev. B **95**, 195202 (2017).

[22]Y. Zhou and M. Hu, "Full quantification of frequency-dependent interfacial thermal conductance contributed by two- and three-phonon scattering processes from nonequilibrium molecular dynamics simulations," Phys. Rev. B **95**, 115313 (2017).

[23]T. Feng, Y. Zhong, J. Shi, and X. Ruan, "Unexpected high inelastic phonon transport across solid-solid interface: Modal nonequilibrium molecular dynamics simulations and Landauer analysis," Phys. Rev. B **99**, 045301 (2019).

[24]Y. X. Xu, H. Z. Fan, and Y. G. Zhou, "Quantifying spectral thermal transport properties in framework of molecular dynamics simulations: A comprehensive review," Rare Metals **42**, 3914–3944 (2023).

[25]N. Yang, T. Luo, K. Esfarjani, A. Henry, Z. Tian, J. Shiomi, Y. Chalopin, B. Li, and G. Chen, "Thermal interface conductance between aluminum and silicon by molecular dynamics simulations," J. Comput. Theor. Nanosci. **12**, 168–174 (2015).

[26]Y. Xu, H. Fan, Z. Li, and Y. Zhou, "Signatures of anharmonic phonon transport in ultrahigh thermal conductance across atomically sharp metal/semiconductor interface," Int. J. Heat Mass Transf. **201**, 123628 (2023).

[27]K. Wu, L. Zhang, D. Wang, F. Li, P. Zhang, L. Sang, M. Liao, K. Tang, J. Ye, and S. Gu, "A comparative study of interfacial thermal conductance between metal and semiconductor," Sci. Rep. **12**, 19907 (2022).

[28]Q. Li, F. Liu, S. Hu, H. Song, S. Yang, H. Jiang, T. Wang, Y. K. Koh, C. Zhao, F. Kang, J. Wu, X. Gu, B. Sun, and X. Wang, "Inelastic phonon transport across atomically sharp metal/semiconductor interfaces," Nat. Commun. **13**, 4901 (2022).

[29]M. Bartkowiak and G. D. Mahan, "Heat and electricity transport through interfaces," Semicond. Semimetals **70**, 245–271 (2001).

[30]P. E. Hopkins, L. M. Phinney, J. R. Serrano, and T. E. Beechem, "Effects of surface roughness and oxide layer on the thermal boundary conductance at aluminum/silicon interfaces," Phys. Rev. B. **82**, 085307 (2010).

[31]A. J. Minnich, J. A. Johnson, A. J. Schmidt, K. Esfarjani, M. S. Dresselhaus, K. A. Nelson, and G. Chen, "Thermal conductivity spectroscopy technique to measure phonon mean free paths," Phys. Rev. Lett. **107**, 095901 (2011).

[32]Y. Chalopin, K. Esfarjani, A. Henry, S. Volz, and G. Chen, "Thermal interface conductance in Si/Ge superlattices by equilibrium molecular dynamics," Phys. Rev. B: Condens. Matter Mater. Phys. **85**, 195302 (2012).

[33]E. S. Landry and A. J. McGaughey, "Thermal boundary resistance predictions from molecular dynamics simulations and theoretical calculations," Phys. Rev. B: Condens. Matter Mater. Phys. **80**, 165304 (2009).

[34]C. Monachon and L. Weber, "Influence of diamond surface termination on thermal boundary conductance between Al and diamond," J. Appl. Phys. **113**, 183504 (2013).

[35]R. B. Wilson and D. G. Cahill, "Anisotropic failure of Fourier theory in time-domain thermoreflectance experiments," Nat. Commun. **5**, 5075 (2014).

[36]B. J. Lee, W. S. Ko, H. K. Kim, and E. H. Kim, "The modified embedded-atom method interatomic potentials and recent progress in atomistic simulations," Calphad **34**, 510–522 (2010).

[37]A. Majumdar and P. Reddy, "Role of electron–phonon coupling in thermal conductance of metal–nonmetal interfaces," Appl. Phys. Lett. **84**, 4768–4770 (2004).

[38]T. Zhan, L. Fang, and Y. Xu, "Prediction of thermal boundary resistance by the machine learning method," Sci. Rep. **7**, 7109 (2017).

[39]S. Ju, T. Shiga, L. Feng, Z. Hou, K. Tsuda, and J. Shiomi, "Designing nanostructures for phonon transport via Bayesian optimization," Phys. Rev. X **7**, 021024 (2017).

[40]P. Roy Chowdhury and X. Ruan, "Unexpected thermal conductivity enhancement in aperiodic superlattices discovered using active machine learning," npj Comput. Mater. **8**, 12 (2022).

[41]Z. Guo, P. Roy Chowdhury, Z. Han, Y. Sun, D. Feng, G. Lin, and X. Ruan, "Fast and accurate machine learning prediction of phonon scattering rates and lattice thermal conductivity," npj Comput. Mater. **9**, 95 (2023).

[42]J. Behler and M. Parrinello, "Generalized neural-network representation of high-dimensional potential-energy surfaces," Phys. Rev. Lett. **98**, 146401 (2007).

[43]A. P. Bartók, M. C. Payne, R. Kondor, and G. Csányi, "Gaussian approximation potentials: The accuracy of quantum mechanics, without the electrons," Phys. Rev. Lett. **104**, 136403 (2010).

[44]A. V. Shapeev, "Moment tensor potentials: A class of systematically improvable interatomic potentials," SIAM J. Multiscale Model. Simul. **14**, 1153–1173 (2016).

[45]A. P. Thompson, L. P. Swiler, C. R. Trott, S. M. Foiles, and G. J. Tucker, "Spectral neighbor analysis method for automated generation of quantum-accurate interatomic potentials," J. Comput. Phys. **285**, 316–330 (2015).

[46]H. Wang, L. Zhang, and J. Han, "DeePMD-kit: A deep learning package for many-body potential energy representation and molecular dynamics," Comp. Phys. Comm. **228**, 178–184 (2018).

[47]J. Behler and G. Csányi, "Machine learning potentials for extended systems: A perspective," Eur. Phys. J. B **94**, 142 (2021).

[48]P. Zhang, Z. Zhang, Y. Liu, Z. Wang, Z. Lu, and R. Xiong, "Phonon thermal transport in Bi_2Te_3 from a deep-neural-network interatomic potential," Phys. Rev. Appl. **18**, 054022 (2022).

[49]R. Li, Z. Liu, A. Rohskopf, K. Gordiz, A. Henry, E. Lee, and T. Luo, "A deep neural network interatomic potential for studying thermal conductivity of β-Ga_2O_3," Appl. Phys. Lett. **117**, 152102 (2020).

[50]C. Mangold, S. Chen, G. Barbalinardo, J. Behler, P. Pochet, K. Termentzidis, Y. Han, L. Chaput, D. Lacroix, and D. Donadio, "Transferability of neural network potentials for varying stoichiometry: Phonons and thermal conductivity of Mn_xGe_y compounds," J. Appl. Phys. **127**, 244901 (2020).

[51]X. Qian, S. Peng, X. Li, Y. Wei, and R. Yang, "Thermal conductivity modeling using machine learning potentials: Application to crystalline and amorphous silicon," Mater. Today Phys. **10**, 100140 (2019).

[52]R. Li, E. Lee, and T. Luo, "A unified deep neural network potential capable of predicting thermal conductivity of silicon in different phases," Mater. Today Phys. **12**, 100181 (2020).

[53]G. Pan, J. Ding, Y. Du, D. J. Lee, and Y. Lu, "A DFT accurate machine learning description of molten $ZnCl_2$ and its mixtures: 2. Potential development and properties prediction of $ZnCl_2$-NaCl-KCl ternary salt for CSP," Comput. Mater. Sci. **187**, 110055 (2021).

[54]P. Korotaev, I. Novoselov, A. Yanilkin, and A. Shapeev, "Accessing thermal conductivity of complex compounds by machine learning interatomic potentials," Phys. Rev. B **100**, 144308 (2019).

[55]J. Tang, G. Li, Q. Wang, J. Zheng, L. Cheng, and R. Guo, "Competition between phonon-vacancy and four-phonon scattering in cubic boron arsenide by machine learning interatomic potential," Phys. Rev. Mater. **7**, 44601 (2023).

[56]J. Tang, G. Li, Q. Wang, J. Zheng, L. Cheng, and R. Guo, "Effect of four-phonon scattering on anisotropic thermal transport in bulk hexagonal boron nitride by machine learning interatomic potential," Int. J. Heat Mass Transf. **207**, 124011 (2023).

[57]X. Liu, B. Wang, K. Jia, Q. Wang, D. Wang, and Y. Xiong, "First-principles-based machine learning interatomic potential for molecular dynamics simulations of 2D lateral MoS_2/WS_2 heterostructures," J. Appl. Phys. **135**, 205107 (2024).

[58]Z. Cheng, R. Li, X. Yan, G. Jernigan, J. Shi, M. E. Liao, N. J. Hines, C. A. Gadre, J. Carlos Idrobo, E. Lee, K. D. Hobart, M. S. Goorsky, X. Pan, T. Luo, and S. Graham, "Experimental observation of localized interfacial phonon modes," Nat. Commun. **12**, 6901 (2021).

[59]P. Zhang, M. Qin, Z. Zhang, D. Jin, Y. Liu, Z. Wang, Z. Lu, J. Shi, and R. Xiong, "Accessing the thermal conductivities of Sb_2Te_3 and Bi_2Te_3/Sb_2Te_3 superlattices by molecular dynamics simulations with a deep neural network potential," Phys. Chem. Chem. Phys. **25**, 6164–6174 (2023).

[60]G. Kresse and J. Furthmüller, "Efficient iterative schemes for *ab initio* total-energy calculations using a plane-wave basis set," Phys. Rev. B **54**, 11169 (1996).

[61]G. Kresse and D. Joubert, "From ultrasoft pseudopotentials to the projector augmented-wave method," Phys. Rev. B **59**, 1758 (1999).

22 March 2025 09:29:40

[62]P. E. Blöchl, "Projector augmented-wave method," Phys. Rev. B **50**, 17953 (1994).

[63]J. P. Perdew, K. Burke, and M. Ernzerhof, "Generalized gradient approximation made simple," Phys. Rev. Lett. **77**, 3865 (1996).

[64]J. Zeng, *et al.*, "DeePMD-kit v2: A software package for deep potential models," J. Chem. Phys. **159**, 054801 (2023).

[65]K. Khot and X. Ruan, GitHub repository (2024); see https://github.com/krutarth24/Al-Si-DeePMD-NNP/.

[66]S. Plimpton, "Fast parallel algorithms for short-range molecular dynamics," J. Comput. Phys. **117**, 1–19 (1995).

[67]A. P. Thompson, H. M. Aktulga, R. Berger, D. S. Bolintineanu, W. M. Brown, P. S. Crozier, A. Kohlmeyer, S. G. Moore, T. D. Nguyen, R. Shan, M. J. Stevens, J. Tranchida, C. Trott, and S. J. Plimpton, "LAMMPS—A flexible simulation tool for particle-based materials modeling at the atomic, meso, and continuum scales," Comput. Phys. Commun. **271**, 108171 (2022).

[68]A. Togo, "First-principles phonon calculations with phonopy and phono3py," J. Phys. Soc. Jpn. **92**, 012001 (2022).

[69]A. Togo, L. Chaput, T. Tadano, and I. Tanaka, "Implementation strategies in phonopy and phono3py," J. Phys.: Condens. Matter **35**, 353001 (2023).

[70]R. R. Zope and Y. Mishin, "Interatomic potentials for atomistic simulations of the Ti-Al system," Phys. Rev. B **68**, 024102 (2003).

[71]A. K. Rappé, C. J. Casewit, K. S. Colwell, W. A. Goddard, and W. M. Skiff, "UFF, a full periodic table force field for molecular mechanics and molecular dynamics simulations," J. Am. Chem. Soc. **114**, 10024–10035 (1992).

[72]J. Tersoff, "Modeling solid-state chemistry: Interatomic potentials for multicomponent systems," Phys. Rev. B **39**, 5566 (1989).

[73]G. Dolling and S. Ekland, *Inelastic Scattering of Neurons in Solids and Liquids* (International Atomic Energy Agency (IAEA), 1963).

[74]R. Stedman and G. Nilsson, "Dispersion relations for phonons in aluminum at 80 and 300 K," Phys. Rev. **145**, 492–500 (1966).

[75]T. Tadano, Y. Gohda, and S. Tsuneyuki, "Anharmonic force constants extracted from first-principles molecular dynamics: Applications to heat transfer simulations," J. Phys.: Condens. Matter **26**, 225402 (2014).

[76]P. K. Schelling, S. R. Phillpot, and P. Keblinski, "Comparison of atomic-level simulation methods for computing thermal conductivity," Phys. Rev. B **65**, 144306 (2002).

[77]H. C. Chien, D. J. Yao, and C. T. Hsu, "Measurement and evaluation of the interfacial thermal resistance between a metal and a dielectric," Appl. Phys. Lett. **93**, 231910 (2008).

[78]Z. Lin, L. V. Zhigilei, and V. Celli, "Electron-phonon coupling and electron heat capacity of metals under conditions of strong electron-phonon nonequilibrium," Phys. Rev. B: Condens. Matter Mater. Phys. **77**, 075133 (2008).

[79]Z. Tong, S. Li, X. Ruan, and H. Bao, "Comprehensive first-principles analysis of phonon thermal conductivity and electron-phonon coupling in different metals," Phys. Rev. B **100**, 144306 (2019).

[80]A. Jain and A. J. McGaughey, "Thermal transport by phonons and electrons in aluminum, silver, and gold from first principles," Phys. Rev. B **93**, 081206 (2016).

[81]W. Bao, Z. Wang, and D. Tang, "Phonon transport across GaN/AlN interface: Interfacial phonon modes and phonon local non-equilibrium analysis," Int. J. Heat Mass Transf. **183**, 122090 (2022).

[82]R. Anufriev, J. Ordonez-Miranda, and M. Nomura, "Measurement of the phonon mean free path spectrum in silicon membranes at different temperatures using arrays of nanoslits," Phys. Rev. B **101**, 115301 (2020).